Nonlocal energy density functionals for pairing and beyond-mean-field calculations

Bennaceur, K.

2017-04

Bennaceur , K , Idini , A , Dobaczewski , J , Dobaczewski , P , Kortelainen , M & Raimondi , F 2017 , ' Nonlocal energy density functionals for pairing and beyond-mean-field calculations ' , Journal of Physics G: Nuclear and Particle Physics , vol. 44 , no. 4 , 045106 . https://doi.org/10.1088/1361-6471/aa

http://hdl.handle.net/10138/307512
https://doi.org/10.1088/1361-6471/aa5fd7

other
acceptedVersion

Nonlocal energy density functionals for pairing and beyond-mean-field calculations

K. Bennaceur[1,2,3], A. Idini[2,4], J. Dobaczewski[2,3,5,6], P. Dobaczewski[7], M. Kortelainen[2,3], and F. Raimondi[2,4]

[1]Univ Lyon, Université Lyon 1, CNRS/IN2P3, IPNL, F-69622 Villeurbanne, France
[2]Department of Physics, PO Box 35 (YFL), FI-40014 University of Jyväskylä, Finland
[3]Helsinki Institute of Physics, P.O. Box 64, FI-00014 University of Helsinki, Finland
[4]Department of Physics, University of Surrey, Guildford GU2 7XH, United Kingdom
[5]Department of Physics, University of York, Heslington, York YO10 5DD, United Kingdom
[6]Institute of Theoretical Physics, Faculty of Physics, University of Warsaw, ul. Pasteura 5, PL-02-093 Warsaw, Poland
[7]ul. Obozowa 85 m. 5, PL-01425 Warsaw, Poland

Abstract. We propose to use two-body regularized finite-range pseudopotential to generate nuclear energy density functional (EDF) in both particle-hole and particle-particle channels, which makes it free from self-interaction and self-pairing, and also free from singularities when used beyond mean field. We derive a sequence of pseudopotentials regularized up to next-to-leading order (NLO) and next-to-next-to-leading order (N^{2}LO), which fairly well describe infinite-nuclear-matter properties and finite open-shell paired and/or deformed nuclei. Since pure two-body pseudopotentials cannot generate sufficiently large effective mass, the obtained solutions constitute a preliminary step towards future implementations, which will include, e.g., EDF terms generated by three-body pseudopotentials.

1. Introduction

The two most widely used families of non-relativistic nuclear energy density functionals (EDFs) are based on the Skyrme [1, 2] and Gogny [3] functional generators. The main difference between them is that the Skyrme-type generators are built as sums of contact terms with nonlocal gradient corrections, whereas the Gogny-type ones are built as sums of local finite-range Gaussians. In Gogny and most Skyrme parametrizations, to conveniently reproduce properties of homogeneous nuclear matter, a two-body density-dependent generator is usually used, most often with a fractional power of the density. Unfortunately, such an approach leads to non-analytic properties of beyond-mean-field EDF in the complex plane [4], compromises symmetry-restoration procedures [5, 4, 6], and introduces self-interaction contributions in the particle-vibration coupling vertex [7].

Thus, to gain progress in the development of a consistent description of atomic nucleus, there clearly appears a need to build EDFs that are free from the above spuriousities. Such functionals can be obtained by defining their potential parts as Hartree-Fock-Bogolyubov (HFB) expectation values of genuine pseudopotential operators. In fact, this was the original idea of Skyrme who first introduced the name pseudopotential in this context [8]. Without density-dependent terms and taking all exchange and pairing terms into account, this gives EDFs for which the Pauli principle is strictly obeyed and removes all spurious contributions. Following Refs. [9, 10], also here we call such pseudopotentials EDF generators.

In Refs. [11, 12, 13, 9], we have already fully developed the formalism that uses contact and regularized higher-order pseudopotentials to generate the most general terms in the EDF compatible with symmetries. There were several recent attempts to use such EDFs, like the development of the Skyrme–inspired family of functionals SLyMR which include 3- and 4-body terms [14], our previous parametrization of the regularized finite-range pseudopotential REG2 [15], or functional VLyB, which implemented higher-order contact terms [16]. However none of the previous attempts managed to reproduce both bulk and pairing properties of finite nuclei, while ensuring at the same time stability of homogeneous nuclear matter.

The aim of this article is thus to present a further step in the construction of a predictive pseudopotential-based EDF. We present an adjustment of a parametrization of the regularized finite-range higher-order local and density-independent pseudopotential, which achieves an acceptable qualitative description both in the particle-hole and particle-particle channels without leading to infinite-matter instabilities. With the limitation of the current implementation being only purely two-body and local, a sufficiently high value of the infinite-matter effective mass could not be obtained. However, reasonably good results obtained for bulk and pairing properties of finite nuclei demonstrate proof-of-principle feasibility of such program.

The article is organized as follows. In section 2 we briefly recall the form of the pseudopotential and present the corresponding EDF terms in particle-hole and particle-particle channels. The numerical implementation of the mean-field equations in the

new HFB spherical solver FINRES$_4$ is briefly discussed in section 3. The strategy used to adjust the parameters is given in section 4. In section 5 we discuss statistical errors of the resulting parameters and observables, and present selected results for infinite nuclear matter and finite nuclei. Conclusions are given in section 6.

2. Regularized pseudopotential

In this section we recall the Cartesian form of the regularized pseudopotential as introduced in [13, 9]. We derived the corresponding EDF both in the particle-hole and particle-particle channels up to N^{3}LO, whereas below we show them up to NLO.

2.1. Form factors of the pseudopotential

The pseudopotential can be regarded as a modified Skyrme interaction with the δ form factor replaced by a finite-range regulator, for which we have chosen a Gaussian form,

$$g_a(\mathbf{r}) = \frac{1}{(a\sqrt{\pi})^3}\,\mathrm{e}^{-\frac{\mathbf{r}^2}{a^2}}\,. \tag{1}$$

The pseudopotential regularized at order p, that is, up to N^{p}LO, depends on differential operators of the order $n = 2p$, and reads

$$\begin{aligned}\mathcal{V}_j^{(n)}(\mathbf{r}_1,\mathbf{r}_2;\mathbf{r}_3,\mathbf{r}_4) = {} & \Big(W_j^{(n)}\hat{1}_\sigma\hat{1}_\tau + B_j^{(n)}\hat{1}_\tau\hat{P}^\sigma - H_j^{(n)}\hat{1}_\sigma\hat{P}^\tau - M_j^{(n)}\hat{P}^\sigma\hat{P}^\tau\Big) \\ & \times \hat{O}_j^{(n)}(\mathbf{k}_{12},\mathbf{k}_{34})\delta(\mathbf{r}_{13})\delta(\mathbf{r}_{24})g_a(\mathbf{r}_{12})\,.\end{aligned} \tag{2}$$

where $\hat{1}_\sigma$ and $\hat{1}_\tau$ are respectively the identity operators in spin and isospin space and $\hat{P}^\sigma$ and $\hat{P}^\tau$ the spin and isospin exchange operators. Standard relative-momentum operators are defined as $\mathbf{k}_{ij} = \frac{1}{2i}(\boldsymbol{\nabla}_i - \boldsymbol{\nabla}_j)$ and relative positions as $\mathbf{r}_{ij} = \mathbf{r}_i - \mathbf{r}_j$. Operators $\hat{O}_j^{(n)}(\mathbf{k}_{12},\mathbf{k}_{34})$ are scalars built at a given order n from relative momenta $\mathbf{k}_{12}^*$ and $\mathbf{k}_{34}$ and index j enumerates such different scalars [9]. We note here that coupling constants $W_j^{(n)}$, $B_j^{(n)}$, $H_j^{(n)}$, and $M_j^{(n)}$ are defined in a different convention than those of the Gogny effective interaction [3], because they include coefficient $(a\sqrt{\pi})^{-3}$ introduced in the form factor in Eq. (1).

At LO, that is for $n = 0$, we have $O_0(\mathbf{k}_{12},\mathbf{k}_{34}) = \hat{1}$, which gives a local pseudopotential that reads,

$$\begin{aligned}\mathcal{V}_{\mathrm{loc}}^{(0)}(\mathbf{r}_1,\mathbf{r}_2;\mathbf{r}_3,\mathbf{r}_4) = {} & \Big(W_1^{(0)}\hat{1}_\sigma\hat{1}_\tau + B_1^{(0)}\hat{1}_\tau\hat{P}^\sigma - H_1^{(0)}\hat{1}_\sigma\hat{P}^\tau - M_1^{(0)}\hat{P}^\sigma\hat{P}^\tau\Big) \\ & \times \delta(\mathbf{r}_{13})\delta(\mathbf{r}_{24})g_a(\mathbf{r}_{12})\,,\end{aligned} \tag{3}$$

At a given order higher order $n > 0$, the pseudopotential is local if it only depends on $\mathbf{k}_{34} + \mathbf{k}_{12} \equiv \mathbf{k}_{34} - \mathbf{k}_{12}^*$ [13, 9]. With the conventions introduced in [9], this corresponds to conditions,

$$\begin{aligned}&W_2^{(n)} = -W_1^{(n)}, \quad B_2^{(n)} = -B_1^{(n)}, \quad H_2^{(n)} = -H_1^{(n)}, \quad M_2^{(n)} = -M_1^{(n)}, \\ &W_j^{(n)} = B_j^{(n)} = H_j^{(n)} = M_j^{(n)} = 0 \quad \text{for} \quad j > 2.\end{aligned} \tag{4}$$

The pseudopotential then takes the form

$$\mathcal{V}_{\rm loc}^{(n)}(\mathbf{r}_1,\mathbf{r}_2;\mathbf{r}_3,\mathbf{r}_4) = \left(W_1^{(n)}\hat{1}_\sigma\hat{1}_\tau + B_1^{(n)}\hat{1}_\tau\hat{P}^\sigma - H_1^{(n)}\hat{1}_\sigma\hat{P}^\tau - M_1^{(n)}\hat{P}^\sigma\hat{P}^\tau\right) \times \left[\hat{O}_1^{(n)}(\mathbf{k}_{12},\mathbf{k}_{34}) - \hat{O}_2^{(n)}(\mathbf{k}_{12},\mathbf{k}_{34})\right]\delta(\mathbf{r}_{13})\delta(\mathbf{r}_{24})g_a(\mathbf{r}_{12}) \quad (5)$$

or

$$\mathcal{V}_{\rm loc}^{(n)}(\mathbf{r}_1,\mathbf{r}_2;\mathbf{r}_3,\mathbf{r}_4) = \left(W_1^{(n)}\hat{1}_\sigma\hat{1}_\tau + B_1^{(n)}\hat{1}_\tau\hat{P}^\sigma - H_1^{(n)}\hat{1}_\sigma\hat{P}^\tau - M_1^{(n)}\hat{P}^\sigma\hat{P}^\tau\right) \times \left(\frac{1}{2}\right)^{n/2}\left[\mathbf{k}_{34}+\mathbf{k}_{12}\right]^n\delta(\mathbf{r}_{13})\delta(\mathbf{r}_{24})g_a(\mathbf{r}_{12})\,. \quad (6)$$

The fact that the derivative operator commutes with $\delta(\mathbf{r}_{13})\delta(\mathbf{r}_{24})$ leads in this case to the following expression

$$\mathcal{V}_{\rm loc}^{(n)}(\mathbf{r}_1,\mathbf{r}_2;\mathbf{r}_3,\mathbf{r}_4) = \left(W_1^{(n)}\hat{1}_\sigma\hat{1}_\tau + B_1^{(n)}\hat{1}_\tau\hat{P}^\sigma - H_1^{(n)}\hat{1}_\sigma\hat{P}^\tau - M_1^{(n)}\hat{P}^\sigma\hat{P}^\tau\right) \times \delta(\mathbf{r}_{13})\delta(\mathbf{r}_{24})\left(\frac{1}{2}\right)^{n/2}\mathbf{k}_{12}^n g_a(\mathbf{r}_{12})\,. \quad (7)$$

Furthermore, the identity,

$$\left(\frac{1}{2i^2}\right)^{n/2}\boldsymbol{\nabla}^n g_a(\mathbf{r}) = \left(-\frac{1}{2}\right)^p\Delta^p g_a(\mathbf{r}) = \left(-\frac{1}{a}\frac{\partial}{\partial a}\right)^p g_a(\mathbf{r})\,, \quad (8)$$

where $p = n/2$, shows that, in the case of a local pseudopotential (4), any contribution to the energy or mean-field regularized at order p can be obtained from the corresponding expression at order $p = 0$ by iterating p times operator $-\frac{1}{a}\frac{\partial}{\partial a}$ on it .

The notations used in this section are suitable for writing the pseudopotential and the corresponding functional at any order. In section 2.2, we restrict the pseudopotential to terms up to second only and adopt a lighter notation with $\mathcal{V}_1^{(0)} \equiv \mathcal{V}_0$, $\mathcal{V}_1^{(2)} \equiv \mathcal{V}_1$, $\mathcal{V}_2^{(2)} \equiv \mathcal{V}_2$ and similar conventions for operators $\hat{O}_j^{(n)}$ and parameters $W_j^{(n)}$, $B_j^{(n)}$, $H_j^{(n)}$ and $M_j^{(n)}$, so we write,

$$\mathcal{V}_k(\mathbf{r}_1,\mathbf{r}_2;\mathbf{r}_3,\mathbf{r}_4) = \left(W_k\hat{1}_\sigma\hat{1}_\tau + B_k\hat{1}_\tau\hat{P}^\sigma - H_k\hat{1}_\sigma\hat{P}^\tau - M_k\hat{P}^\sigma\hat{P}^\tau\right) \times \hat{O}_k(\mathbf{k}_{12},\mathbf{k}_{34})\delta(\mathbf{r}_{13})\delta(\mathbf{r}_{24})g_a(\mathbf{r}_{12})\,, \quad (9)$$

with $k = 0$, 1, or 2.

2.1.1. Nonlocal densities and currents. An average value of the energy of a nucleus can be conveniently written using one-body normal and pairing densities. Their definitions and some properties [17] are recalled in this section.

For a given reference state $|\Psi\rangle$, the non-local one-body (normal) density is defined as

$$\rho(\mathbf{r}_1 s_1 t_1, \mathbf{r}_2 s_2 t_2) = \langle\Psi|a^\dagger_{\mathbf{r}_2 s_2 t_2} a_{\mathbf{r}_1 s_1 t_1}|\Psi\rangle\,, \quad (10)$$

where the operators $a^\dagger_{\mathbf{r}st}$ and $a_{\mathbf{r}st}$ create and annihilate nucleons at position $\mathbf{r}$ having spin and isospin projections $s = \pm\frac{1}{2}$ and $t = \pm\frac{1}{2}$. The pairing density is defined as

$$\tilde{\rho}(\mathbf{r}_1 s_1 t_1, \mathbf{r}_2 s_2 t_2) = -2s_2\langle\Psi|a_{\mathbf{r}_2 -s_2 t_2} a_{\mathbf{r}_1 s_1 t_1}|\Psi\rangle\,. \quad (11)$$

These two densities satisfy the properties

$$\rho(\mathbf{r}_1 s_1 t_1, \mathbf{r}_2 s_2 t_2) = \rho^*(\mathbf{r}_2 s_2 t_2, \mathbf{r}_1 s_1 t_1)\,, \tag{12}$$

$$\tilde{\rho}(\mathbf{r}_1 s_1 t_1, \mathbf{r}_2 s_2 t_2) = 4 s_1 s_2\, \tilde{\rho}(\mathbf{r}_2\text{-}s_2 t_2, \mathbf{r}_1\text{-}s_1 t_1)\,. \tag{13}$$

In the present article, we do not consider the possibility to mix protons and neutrons. This restriction has the consequence that the normal and pairing densities are diagonal in the neutron-proton space. In this situation, the normal density can be expanded in (iso)scalar/(iso)vector parts using identity and Pauli matrices as

$$\begin{aligned}\rho(\mathbf{r}_1 s_1 t_1, \mathbf{r}_2 s_2 t_2) = {} & \tfrac{1}{4}\,\rho_0(\mathbf{r}_1, \mathbf{r}_2)\delta_{s_1 s_2}\delta_{t_1 t_2} + \tfrac{1}{4}\,\rho_1(\mathbf{r}_1, \mathbf{r}_2)\delta_{s_1 s_2}\tau^{(3)}_{t_1 t_2} \\ & + \tfrac{1}{4}\,\mathbf{s}_0(\mathbf{r}_1, \mathbf{r}_2)\cdot\boldsymbol{\sigma}_{s_1 s_2}\delta_{t_1 t_2} + \tfrac{1}{4}\,\mathbf{s}_1(\mathbf{r}_1, \mathbf{r}_2)\cdot\boldsymbol{\sigma}_{s_1 s_2}\tau^{(3)}_{t_1 t_2}\,,\end{aligned} \tag{14}$$

and the pairing density as

$$\tilde{\rho}(\mathbf{r}_1 s_1 t, \mathbf{r}_2 s_2 t) = \tfrac{1}{2}\,\tilde{\rho}_t(\mathbf{r}_1, \mathbf{r}_2)\delta_{s_1 s_2} + \tfrac{1}{2}\,\tilde{\mathbf{s}}_t(\mathbf{r}_1, \mathbf{r}_2)\cdot\boldsymbol{\sigma}_{s_1 s_2}\,. \tag{15}$$

In the latter expression, index $t = n$ or p stands for neutrons or protons, respectively.

Since the pseudopotential may contain derivative terms, we introduce the following nonlocal densities

$$\tau_T(\mathbf{r}_1, \mathbf{r}_2) = \boldsymbol{\nabla}_1\cdot\boldsymbol{\nabla}_2\,\rho_T(\mathbf{r}_1, \mathbf{r}_2)\,, \tag{16}$$

$$\mathbf{T}_T(\mathbf{r}_1, \mathbf{r}_2) = \boldsymbol{\nabla}_1\cdot\boldsymbol{\nabla}_2\,\mathbf{s}_T(\mathbf{r}_1, \mathbf{r}_2)\,, \tag{17}$$

$$\mathbf{j}_T(\mathbf{r}_1, \mathbf{r}_2) = \tfrac{1}{2\mathrm{i}}\,(\boldsymbol{\nabla}_1 - \boldsymbol{\nabla}_2)\,\rho_T(\mathbf{r}_1, \mathbf{r}_2)\,, \tag{18}$$

$$J_{T\mu\nu}(\mathbf{r}_1, \mathbf{r}_2) = \tfrac{1}{2\mathrm{i}}\,(\boldsymbol{\nabla}_1 - \boldsymbol{\nabla}_2)_\mu\,s_{T\nu}(\mathbf{r}_1, \mathbf{r}_2) \tag{19}$$

which are respectively the nonlocal scalar kinetic, pseudo-vector spin-kinetic, vector current and spin-orbit tensor densities. In these expressions, index $T = 0$ or 1 stands for isoscalar or isovector densities, respectively and μ and ν represent the Cartesian coordinates in directions x, y and z. In a similar manner, we introduce the following non-local pairing densities

$$\tilde{\tau}_t(\mathbf{r}_1, \mathbf{r}_2) = \boldsymbol{\nabla}_1\cdot\boldsymbol{\nabla}_2\,\tilde{\rho}_t(\mathbf{r}_1, \mathbf{r}_2)\,, \tag{20}$$

$$\tilde{\mathbf{T}}_t(\mathbf{r}_1, \mathbf{r}_2) = \boldsymbol{\nabla}_1\cdot\boldsymbol{\nabla}_2\,\tilde{\mathbf{s}}_t(\mathbf{r}_1, \mathbf{r}_2)\,, \tag{21}$$

$$\tilde{\boldsymbol{j}}_t(\mathbf{r}_1, \mathbf{r}_2) = \tfrac{1}{2\mathrm{i}}\,(\boldsymbol{\nabla}_1 - \boldsymbol{\nabla}_2)\,\tilde{\rho}_t(\mathbf{r}_1, \mathbf{r}_2)\,, \tag{22}$$

$$\tilde{J}_{t\mu\nu}(\mathbf{r}_1, \mathbf{r}_2) = \tfrac{1}{2\mathrm{i}}\,(\boldsymbol{\nabla}_1 - \boldsymbol{\nabla}_2)_\mu\,\tilde{s}_{t\nu}(\mathbf{r}_1, \mathbf{r}_2)\,. \tag{23}$$

2.2. Structure of the nonlocal energy density functional

By summing over spin and isospin indices, one obtains contributions to the energy that come from different terms of the regularized pseudopotential, as given in equation (9). For given values of k, this energy contains the local part,

$$\begin{aligned}\langle V_k^L\rangle = {} & \sum_{T=0,1}\int \mathrm{d}^3 r_1\,\mathrm{d}^3 r_2\,\mathrm{d}^3 r_3\,\mathrm{d}^3 r_4\,\Big[\hat{O}_k(\mathbf{k}_{12}, \mathbf{k}_{34})\delta(\mathbf{r}_{13})\delta(\mathbf{r}_{24})g_a(\mathbf{r}_{12})\Big] \\ & \times\Big[A_k^{\rho_T}\rho_T(\mathbf{r}_3, \mathbf{r}_1)\rho_T(\mathbf{r}_4, \mathbf{r}_2) + A_k^{\mathbf{s}_T}\mathbf{s}_T(\mathbf{r}_3, \mathbf{r}_1)\cdot\mathbf{s}_T(\mathbf{r}_4, \mathbf{r}_2)\Big]\,,\end{aligned} \tag{24}$$

the nonlocal part,

$$\langle V_k^N \rangle = \sum_{T=0,1} \int \mathrm{d}^3r_1\, \mathrm{d}^3r_2\, \mathrm{d}^3r_3\, \mathrm{d}^3r_4 \left[\hat{O}_k(\mathbf{k}_{12},\mathbf{k}_{34})\delta(\mathbf{r}_{13})\delta(\mathbf{r}_{24})g_a(\mathbf{r}_{12})\right] \times \left[B_k^{\rho_T}\rho_T(\mathbf{r}_4,\mathbf{r}_1)\rho_T(\mathbf{r}_3,\mathbf{r}_2) + B_k^{\mathbf{s}_T}\mathbf{s}_T(\mathbf{r}_4,\mathbf{r}_1)\cdot\mathbf{s}_T(\mathbf{r}_3,\mathbf{r}_2)\right], \tag{25}$$

and the pairing part

$$\langle V_k^P \rangle = \sum_{t=n,p} \int \mathrm{d}^3r_1\, \mathrm{d}^3r_2\, \mathrm{d}^3r_3\, \mathrm{d}^3r_4 \left[\hat{O}_k(\mathbf{k}_{12},\mathbf{k}_{34})\delta(\mathbf{r}_{13})\delta(\mathbf{r}_{24})g_a(\mathbf{r}_{12})\right] \times \left[C_k^{\tilde{\rho}}\,\tilde{\rho}_t^*(\mathbf{r}_1,\mathbf{r}_2)\tilde{\rho}_t(\mathbf{r}_3,\mathbf{r}_4) + C_k^{\tilde{\mathbf{s}}}\,\tilde{\mathbf{s}}_t^*(\mathbf{r}_1,\mathbf{r}_2)\cdot\tilde{\mathbf{s}}_t(\mathbf{r}_3,\mathbf{r}_4)\right]. \tag{26}$$

Expressions for coupling constants A, B, and C that appear in Eqs. (24), (25), and (26) read

$$A_k^{\rho 0} = \tfrac{1}{2}W_k + \tfrac{1}{4}B_k - \tfrac{1}{4}H_k - \tfrac{1}{8}M_k\,, \tag{27}$$
$$A_k^{\mathbf{s}0} = \tfrac{1}{4}B_k - \tfrac{1}{8}M_k\,, \tag{28}$$
$$B_k^{\rho 0} = -\tfrac{1}{8}W_k - \tfrac{1}{4}B_k + \tfrac{1}{4}H_k + \tfrac{1}{2}M_k\,, \tag{29}$$
$$B_k^{\mathbf{s}0} = -\tfrac{1}{8}W_k + \tfrac{1}{4}H_k\,, \tag{30}$$
$$A_k^{\rho 1} = -\tfrac{1}{4}H_k - \tfrac{1}{8}M_k\,, \tag{31}$$
$$A_k^{\mathbf{s}1} = -\tfrac{1}{8}M_k\,, \tag{32}$$
$$B_k^{\rho 1} = -\tfrac{1}{8}W_k - \tfrac{1}{4}B_k\,, \tag{33}$$
$$B_k^{\mathbf{s}1} = -\tfrac{1}{8}W_k\,, \tag{34}$$
$$C_k^{\tilde{\rho}} = \tfrac{1}{4}W_k - \tfrac{1}{4}B_k - \tfrac{1}{4}H_k + \tfrac{1}{4}M_k\,, \tag{35}$$
$$C_k^{\tilde{\mathbf{s}}} = \tfrac{1}{4}W_k + \tfrac{1}{4}B_k - \tfrac{1}{4}H_k - \tfrac{1}{4}M_k\,. \tag{36}$$

2.2.1. Leading-order term of the pseudopotential. The leading-order pseudopotential is modeled by a simple Gaussian form factor and does not contain derivative terms. In this case, operator $\hat{O}_0$ simply reads

$$\hat{O}_0(\mathbf{k}_{12},\mathbf{k}_{34}) = \hat{1}\,, \tag{37}$$

and Eqs. (24), (25), and (26) become

$$\langle V_0^L \rangle = \sum_{T=0,1} \int \mathrm{d}^3r_1\, \mathrm{d}^3r_2\, g_a(\mathbf{r}_{12}) \Big[A_0^{\rho_T}\rho_T(\mathbf{r}_1)\rho_T(\mathbf{r}_2) + A_0^{\mathbf{s}_T}\mathbf{s}_T(\mathbf{r}_1)\cdot\mathbf{s}_T(\mathbf{r}_2)\Big], \tag{38}$$

$$\langle V_0^N \rangle = \sum_{T=0,1} \int \mathrm{d}^3r_1\, \mathrm{d}^3r_2\, g_a(\mathbf{r}_{12}) \Big[B_0^{\rho_T}\rho_T(\mathbf{r}_2,\mathbf{r}_1)\rho_T(\mathbf{r}_1,\mathbf{r}_2) + B_0^{\mathbf{s}_T}\mathbf{s}_T(\mathbf{r}_2,\mathbf{r}_1)\cdot\mathbf{s}_T(\mathbf{r}_1,\mathbf{r}_2)\Big], \tag{39}$$

$$\langle V_0^P \rangle = \sum_{t=n,p} \int \mathrm{d}^3r_1\, \mathrm{d}^3r_2\, g_a(\mathbf{r}_{12}) \Big[C_0^{\tilde{\rho}}\,\tilde{\rho}_t^*(\mathbf{r}_1,\mathbf{r}_2)\tilde{\rho}_t(\mathbf{r}_1,\mathbf{r}_2) + C_0^{\tilde{\mathbf{s}}}\,\tilde{\mathbf{s}}_t^*(\mathbf{r}_1,\mathbf{r}_2)\cdot\tilde{\mathbf{s}}_t(\mathbf{r}_1,\mathbf{r}_2)\Big]. \tag{40}$$

2.2.2. Next-to-leading order term of the pseudopotential At NLO, the two derivative operators are

$$\hat{O}_1(\mathbf{k}_{12},\mathbf{k}_{34}) = \tfrac{1}{2}\left(\mathbf{k}_{12}^{*2}+\mathbf{k}_{34}^{2}\right)\,, \tag{41}$$

and

$$\hat{O}_2(\mathbf{k}_{12},\mathbf{k}_{34}) = \mathbf{k}_{12}^{*}\cdot\mathbf{k}_{34}\,, \tag{42}$$

The contribution from the first one to the EDF is given by

$$\begin{aligned}\langle V_1^L\rangle = \frac{1}{2}\sum_{T=0,1}\int \mathrm{d}^3r_1\,\mathrm{d}^3r_2\,g_a(\mathbf{r}_{12})\\ \times\Big\{A_1^{\rho_T}\Big[\tau_T(\mathbf{r}_1)\rho_T(\mathbf{r}_2)-\tfrac{3}{4}\,\rho_T(\mathbf{r}_1)\Delta_2\rho_T(\mathbf{r}_2)-\mathbf{j}_T(\mathbf{r}_1)\cdot\mathbf{j}_T(\mathbf{r}_2)\Big]\\ + A_1^{\mathbf{s}_T}\Big[\mathbf{T}_T(\mathbf{r}_1)\cdot\mathbf{s}_T(\mathbf{r}_2)-\tfrac{3}{4}\,\mathbf{s}_T(\mathbf{r}_2)\cdot\Delta_1\mathbf{s}_T(\mathbf{r}_1)\\ -\sum_{\mu\nu}J_{T\mu\nu}(\mathbf{r}_1)J_{T\mu\nu}(\mathbf{r}_2)\Big]\Big\}\,,\end{aligned} \tag{43}$$

$$\begin{aligned}\langle V_1^N\rangle = -\frac{1}{2}\sum_{T=0,1}\int \mathrm{d}^3r_1\,\mathrm{d}^3r_2\\ \times\Big\{\frac{1}{2}\Delta g_a(\mathbf{r}_{12})\left[B_1^{\rho_T}\rho_T(\mathbf{r}_2,\mathbf{r}_1)\rho_T(\mathbf{r}_1,\mathbf{r}_2)+B_1^{\mathbf{s}_T}\mathbf{s}_T(\mathbf{r}_2,\mathbf{r}_1)\cdot\mathbf{s}_T(\mathbf{r}_1,\mathbf{r}_2)\right]\\ + B_1^{\rho_T}g_a(\mathbf{r}_{12})\Big[\rho_T(\mathbf{r}_2,\mathbf{r}_1)\tau_T(\mathbf{r}_1,\mathbf{r}_2)+\rho_T(\mathbf{r}_2,\mathbf{r}_1)\Delta_1\rho_T(\mathbf{r}_1,\mathbf{r}_2)\Big]\\ + B_1^{\mathbf{s}_T}g_a(\mathbf{r}_{12})\Big[\mathbf{s}_T(\mathbf{r}_2,\mathbf{r}_1)\cdot\mathbf{T}_T(\mathbf{r}_1,\mathbf{r}_2)+\mathbf{s}_T(\mathbf{r}_2,\mathbf{r}_1)\cdot\Delta_1\mathbf{s}_T(\mathbf{r}_1,\mathbf{r}_2)\Big]\Big\}\,,\end{aligned} \tag{44}$$

and

$$\begin{aligned}\langle V_1^P\rangle = \frac{1}{2}\sum_{t=n,p}\int \mathrm{d}^3r_1\,\mathrm{d}^3r_2\,g_a(\mathbf{r}_{12})\\ \times\Big\{C_1^{\tilde{\rho}}\Big[\tilde{\rho}_t^{*}(\mathbf{r}_1,\mathbf{r}_2)\tilde{\tau}_t(\mathbf{r}_1,\mathbf{r}_2)-\tilde{\rho}_t^{*}(\mathbf{r}_1,\mathbf{r}_2)\Delta_1\tilde{\rho}_t(\mathbf{r}_1,\mathbf{r}_2)\Big]\\ + C_1^{\tilde{\mathbf{s}}}\Big[\tilde{\mathbf{s}}_t^{*}(\mathbf{r}_1,\mathbf{r}_2)\cdot\tilde{\mathbf{T}}_t(\mathbf{r}_1,\mathbf{r}_2)-\tilde{\mathbf{s}}_t^{*}(\mathbf{r}_1,\mathbf{r}_2)\cdot\Delta_1\tilde{\mathbf{s}}_t(\mathbf{r}_1,\mathbf{r}_2)\Big]\Big\}\,,\end{aligned} \tag{45}$$

and in turn the contribution from the second one is

$$\begin{aligned}\langle V_2^L\rangle = \frac{1}{2}\sum_{T=0,1}\int \mathrm{d}^3r_1\,\mathrm{d}^3r_2\,g_a(\mathbf{r}_{12})\\ \times\Big\{A_2^{\rho_T}\Big[\rho_T(\mathbf{r}_1)\tau_T(\mathbf{r}_2)+\tfrac{1}{4}\,\rho_T(\mathbf{r}_1)\Delta_2\rho_T(\mathbf{r}_2)-\mathbf{j}_T(\mathbf{r}_1)\cdot\mathbf{j}_T(\mathbf{r}_2)\Big]\\ + A_2^{\mathbf{s}_T}\Big[\mathbf{s}_T(\mathbf{r}_1)\cdot\mathbf{T}_T(\mathbf{r}_2)+\tfrac{1}{4}\,\mathbf{s}_T(\mathbf{r}_2)\cdot\Delta_1\mathbf{s}_T(\mathbf{r}_1)\\ -\sum_{\mu\nu}J_{T\mu\nu}(\mathbf{r}_1)J_{T\mu\nu}(\mathbf{r}_2)\Big]\Big\}\,,\end{aligned} \tag{46}$$

$$\langle V_2^N\rangle = \frac{1}{2}\sum_{T=0,1}\int \mathrm{d}^3r_1\,\mathrm{d}^3r_2$$

$$\times \Big\{ \frac{1}{2}\Delta g_a(\mathbf{r}_{12}) \left[B_2^{\rho_T} \rho_T(\mathbf{r}_2,\mathbf{r}_1)\rho_T(\mathbf{r}_1,\mathbf{r}_2) + B_2^{\mathbf{s}_T} \mathbf{s}_T(\mathbf{r}_2,\mathbf{r}_1)\cdot\mathbf{s}_T(\mathbf{r}_1,\mathbf{r}_2)\right]$$
$$- B_2^{\rho_T} g_a(\mathbf{r}_{12}) \Big[\rho_T(\mathbf{r}_2,\mathbf{r}_1)\Delta_1\rho_T(\mathbf{r}_1,\mathbf{r}_2) + \rho_T(\mathbf{r}_2,\mathbf{r}_1)\tau_T(\mathbf{r}_1,\mathbf{r}_2)\Big]$$
$$- B_2^{\mathbf{s}_T} g_a(\mathbf{r}_{12}) \Big[\mathbf{s}_T(\mathbf{r}_2,\mathbf{r}_1)\cdot\Delta_1\mathbf{s}_T(\mathbf{r}_1,\mathbf{r}_2) + \mathbf{s}_T(\mathbf{r}_2,\mathbf{r}_1)\cdot\mathbf{T}_T(\mathbf{r}_1,\mathbf{r}_2)\Big] \Big\} \quad (47)$$

and

$$\langle V_2^P \rangle = \frac{1}{2}\sum_{t=n,p}\int \mathrm{d}^3r_1\,\mathrm{d}^3r_2$$
$$\times \Big\{ \Delta g_a(\mathbf{r}_{12}) \Big[C_2^{\tilde\rho}\,\tilde\rho_t^*(\mathbf{r}_1,\mathbf{r}_2)\tilde\rho_t(\mathbf{r}_1,\mathbf{r}_2) + C_2^{\tilde{\mathbf{s}}}\,\tilde{\mathbf{s}}_t^*(\mathbf{r}_1,\mathbf{r}_2)\cdot\tilde{\mathbf{s}}_t(\mathbf{r}_1,\mathbf{r}_2)\Big]$$
$$+ C_2^{\tilde\rho} g_a(\mathbf{r}_{12}) \Big[\tilde\rho_t^*(\mathbf{r}_1,\mathbf{r}_2)\tilde\tau_t(\mathbf{r}_1,\mathbf{r}_2) - \tilde\rho_t^*(\mathbf{r}_1,\mathbf{r}_2)\Delta_1\tilde\rho_t(\mathbf{r}_1,\mathbf{r}_2)\Big]$$
$$+ C_2^{\tilde{\mathbf{s}}} g_a(\mathbf{r}_{12}) \Big[\tilde{\mathbf{s}}_t^*(\mathbf{r}_1,\mathbf{r}_2)\cdot\tilde{\mathbf{T}}_t(\mathbf{r}_1,\mathbf{r}_2) - \tilde{\mathbf{s}}_t^*(\mathbf{r}_1,\mathbf{r}_2)\cdot\Delta_1\tilde{\mathbf{s}}_t(\mathbf{r}_1,\mathbf{r}_2)\Big] \Big\}. \quad (48)$$

2.2.3. Sum of pseudopotential terms at NLO. The sum of the terms at NLO leads to the expression where contributions from the local and nonlocal parts of the pseudopotential can be explicitly separated. This leads to a form where we can take advantage of property (8), and which is therefore simpler to implement numerically.

Before we write down the sum of terms given by the two NLO pseudopotential terms, it is convenient to introduce the following notation for half sum and half difference of the NLO coupling constants, for example

$$A_{12}^{\rho_0} = \frac{1}{2}\left(A_1^{\rho_0} + A_2^{\rho_0}\right), \quad (49)$$
$$A_{\overline{12}}^{\rho_0} = \frac{1}{2}\left(A_1^{\rho_0} - A_2^{\rho_0}\right). \quad (50)$$

This notation allows us to separate terms of the functional that come from the local part of the pseudopotential (parameterized by terms with indices $\overline{12}$) from those that come from the nonlocal part of pseudopotential (parameterized by terms with indices 12). The sum of NLO terms shown in section 2.2.2 then reads

$$\langle V_1^L \rangle + \langle V_2^L \rangle = \sum_{T=0,1}\int \mathrm{d}^3r_1\,\mathrm{d}^3r_2$$
$$\times \Big\{ A_{12}^{\rho_T} g_a(\mathbf{r}_{12}) \Big[\tau_T(\mathbf{r}_1)\rho_T(\mathbf{r}_2) - \tfrac{1}{4}\,\rho_T(\mathbf{r}_1)\Delta_2\rho_T(\mathbf{r}_2) - \mathbf{j}_T(\mathbf{r}_1)\cdot\mathbf{j}_T(\mathbf{r}_2)\Big]$$
$$+ A_{12}^{\mathbf{s}_T} g_a(\mathbf{r}_{12}) \Big[\mathbf{T}_T(\mathbf{r}_1)\cdot\mathbf{s}_T(\mathbf{r}_2) - \tfrac{1}{4}\,\mathbf{s}_T(\mathbf{r}_2)\cdot\Delta_1\mathbf{s}_T(\mathbf{r}_1) - \mathsf{J}_T(\mathbf{r}_1)\cdot\mathsf{J}_T(\mathbf{r}_2)\Big]$$
$$- \frac{1}{2}\Delta g_a(\mathbf{r}_{12}) \left[A_{\overline{12}}^{\rho_T}\rho_T(\mathbf{r}_1)\rho_T(\mathbf{r}_2) + A_{\overline{12}}^{\mathbf{s}_T}\mathbf{s}_T(\mathbf{r}_1)\cdot\mathbf{s}_T(\mathbf{r}_2)\right] \Big\}, \quad (51)$$

$$\langle V_1^N \rangle + \langle V_2^N \rangle = -\sum_{T=0,1}\int \mathrm{d}^3r_1\,\mathrm{d}^3r_2$$
$$\times \Big\{ B_{12}^{\rho_T} g_a(\mathbf{r}_{12}) \Big[\rho_T(\mathbf{r}_2,\mathbf{r}_1)\Delta_1\rho_T(\mathbf{r}_1,\mathbf{r}_2) + \rho_T(\mathbf{r}_2,\mathbf{r}_1)\tau_T(\mathbf{r}_1,\mathbf{r}_2)\Big]$$
$$+ B_{12}^{\mathbf{s}_T} g_a(\mathbf{r}_{12}) \Big[\mathbf{s}_T(\mathbf{r}_2,\mathbf{r}_1)\cdot\Delta_1\mathbf{s}_T(\mathbf{r}_1,\mathbf{r}_2) + \mathbf{s}_T(\mathbf{r}_2,\mathbf{r}_1)\cdot\mathbf{T}_T(\mathbf{r}_1,\mathbf{r}_2)\Big]$$

$$+\frac{1}{2}\,\Delta g_a(\mathbf{r}_{12})\left[B^{\rho_T}_{\overline{12}}\rho_T(\mathbf{r}_2,\mathbf{r}_1)\rho_T(\mathbf{r}_1,\mathbf{r}_2)+B^{\mathbf{s}_T}_{\overline{12}}\mathbf{s}_T(\mathbf{r}_2,\mathbf{r}_1)\cdot\mathbf{s}_T(\mathbf{r}_1,\mathbf{r}_2)\right]\Big\} \quad (52)$$

and

$$\langle V_1^P\rangle+\langle V_2^P\rangle=\sum_{t=n,p}\int \mathrm{d}^3r_1\,\mathrm{d}^3r_2$$
$$\times\Big\{C^{\tilde\rho}_{12}\,g_a(\mathbf{r}_{12})\Big[\tilde\rho^*_t(\mathbf{r}_1,\mathbf{r}_2)\tilde\tau_t(\mathbf{r}_1,\mathbf{r}_2)-\tilde\rho^*_t(\mathbf{r}_1,\mathbf{r}_2)\Delta_1\tilde\rho_t(\mathbf{r}_1,\mathbf{r}_2)\Big]$$
$$+C^{\tilde{\mathbf{s}}}_{12}\,g_a(\mathbf{r}_{12})\Big[\tilde{\mathbf{s}}^*_t(\mathbf{r}_1,\mathbf{r}_2)\cdot\tilde{\mathbf{T}}_t(\mathbf{r}_1,\mathbf{r}_2)-\tilde{\mathbf{s}}^*_t(\mathbf{r}_1,\mathbf{r}_2)\cdot\Delta_1\tilde{\mathbf{s}}_t(\mathbf{r}_1,\mathbf{r}_2)\Big]$$
$$-\frac{1}{2}\,\Delta g_a(\mathbf{r}_{12})\left[C^{\rho}_{\overline{12}}\rho^*_t(\mathbf{r}_1,\mathbf{r}_2)\rho_t(\mathbf{r}_1,\mathbf{r}_2)+C^{\mathbf{s}}_{\overline{12}}\mathbf{s}^*_t(\mathbf{r}_1,\mathbf{r}_2)\cdot\mathbf{s}_t(\mathbf{r}_1,\mathbf{r}_2)\right]\Big\}. \quad (53)$$

One can easily check that when the pseudopotential is reduced to its local part, three Eqs. (51), (52), and (53) can respectively be obtained from Eqs. (38), (39), and (40) by using property (8).

3. Numerical implementations

The use of a finite-range pseudopotential makes the mean-field equations a set of coupled non-linear integro-differential equations, as much as implementing Coulomb interaction exactly and two-body centre-of-mass correction. In this study, we solve this set of equations in spherical symmetry using a newly developed code FINRES$_4$ (Finite-Range Self-consistent Spherical Space-coordinate Solver) [18], which is based on the method proposed by Hooverman [19]. With this method, the differential and integral operators take a form of square matrices, whereas local fields are simply represented by diagonal ones.

Specifically, densities, fields, and wave functions are discretized in a spherical box of radius R on a mesh with spacing δr starting at $r=\delta r/2$. The numerical parameters are then R, δr and $\ell_{\max}$. The latter parameter corresponds to the maximum value of the orbital angular momentum in the partial-wave expansion of one-body nonlocal densities. The boundary values of wave functions are fixed by the finite difference formulae used to calculate their derivatives near $r=R$. In this work, we have chosen to have vanishing wave functions at $r=R$ in all partial waves.

For deformed nuclei, we used code HFODD (v2.78g) [20], that is a new version based on previous releases [21, 22], in which we implemented self-consistent solutions for finite-range higher-order pseudopotentials. Calculations were performed using Cartesian deformed harmonic-oscillator basis with states included up to $N_0=16$ shells.

4. Adjustments of coupling constants

In the present implementation, the regularized finite-range local pseudopotential was supplemented by the Coulomb term and standard zero-range spin-orbit term [23, 2], and, as discussed below, by a zero-range two-body term that acts only in the particle-hole channel. The spin-orbit term was not included in the pairing channel. Effects

of the spurious centre-of-mass motion were approximately removed by the standard technique consisting in subtracting from the functional (before variation and without the one-body approximation) the average value of the momentum squared divided by twice total mass [24]. Adjustments of coupling constants were performed in spherical symmetry. For simplicity, small contributions to pairing terms that come from the spin-orbit interaction were neglected. In addition, for deformed nuclei calculations were performed with contributions to pairing terms that come from the Coulomb term also neglected. These two latter restrictions will be released in future implementations.

Coupling constants of the regularized pseudopotential were determined by building and minimizing a penalty function whose content is discussed below. For a given value of the regularization range a, the regularized finite-range local pseudopotential (4), depends on 8 independent parameters at NLO and on 12 at N^{2}LO. The strength of the spin-orbit interaction makes one additional parameter $W_{\rm SO}$.

After performing several preliminary adjustments, we noted that pairing fields were strongly peaked at the nuclear surface. This feature has two unwanted consequences. Firstly, pairing energies and average gaps were becoming unreasonably strong in neutron rich isotopes, where a neutron skin develops. Secondly, proton pairing gaps were much too weak compared to typical expected values. This was due to the fact that the Coulomb barrier shifts the proton density from the surface to the nuclear interior.

As a solution to these problems, we considered adding to the functional a term that makes pairing stronger in the volume without increasing its strength at the surface. Equivalently, the one which balances the finite-range pseudopotential, so that it can be stronger in the pairing channel, without letting the particle-hole channel becoming too attractive. This can be achieved by adding a zero-range term of the standard Skyrme type,

$$\mathcal{V}_\delta(\mathbf{r}_1,\mathbf{r}_2;\mathbf{r}_3,\mathbf{r}_4) = t_0\left(1+x_0\hat{P}^\sigma\right)\delta(\mathbf{r}_{13})\delta(\mathbf{r}_{24})\delta(\mathbf{r}_{12})\,, \tag{54}$$

with $x_0 = 1$. This zero-range term indeed allows us to de-correlate the behaviour of the LO terms in the particle-hole and $T = 1$ particle-particle channels. Since this term does not act in the pairing channel, no pairing cut-off is needed. However, when used in beyond-mean-field applications, this term may still lead to ultra-violet divergence. In principle, it would be very easy to avoid this by regularizing this term with a short-range regulator. This route may be exploited in future developments.

A series of tests performed at NLO showed that for regularization ranges between $a = 1.1$ and $1.3\,$fm, the value of $t_0 = 1000$ MeV fm^3 leads to a pairing field which is not too strongly peaked at the surface. In order to limit the number of free parameters, this value for t_0 was fixed and kept constant for all pseudopotentials at NLO and N^{2}LO. We note that by adopting a fixed value of parameter t_0, we removed its influence on the error budget discussed in section 5.2.

4.1. The penalty function

The penalty function [25] depends on the vector of parameters of the model $\boldsymbol{p}$,

$$\chi^2(\boldsymbol{p}) = \sum_{i=1}^{N_d} \frac{\left(\mathcal{O}_i(\boldsymbol{p}) - \mathcal{O}_i^{\text{target}}\right)^2}{\Delta\mathcal{O}_i^2}, \tag{55}$$

and measures quadratic deviation between calculated $\mathcal{O}_i(\boldsymbol{p})$ and target $\mathcal{O}_i^{\text{target}}$ values for a set of observables or pseudo-observables with given adopted uncertainties $\Delta\mathcal{O}_i$. In our implementation, we built the penalty function as a sum of six different components,

$$\chi^2 = \chi^2_{\text{inm}} + \chi^2_{\text{pol}} + \chi^2_{\text{BE}} + \chi^2_{\text{rad}} + \chi^2_{\text{gap}} + \chi^2_{\rho_1}, \tag{56}$$

which are defined as follows:

- We constrained the following properties of the saturation point of the infinite nuclear matter, see [15] for definitions, with their adopted uncertainties: saturation density $\rho_{\text{sat}} = 0.160 \pm 0.0005$ fm^{-3}, binding energy per nucleon $E/A = -16.00 \pm 0.05$ MeV, incompressibility modulus $K_\infty = 230 \pm 1$ MeV, symmetry energy $J = 32.0 \pm 0.1$ MeV and its slope $L = 50 \pm 10$ MeV. The sum of contributions from these properties to the penalty function is denoted χ^2_{inm}.
- One value for the energy per nucleon in polarized matter $B_\uparrow(0.16) = 35 \pm 1$ MeV. This value does not correspond to the result from a microscopic calculation and is only considered to prevent the collapse of polarized matter near the saturation point. We denote the contribution from this constraint to the penalty function as χ^2_{pol}.
- Binding energies and proton radii of several doubly magic and semi-magic nuclei as summarized in Table 1. Contributions to the penalty function from theses quantities are denoted χ^2_{BE} and χ^2_{rad}, respectively.
- The zero-range term (54) turned out to be useful but not sufficient to guarantee that the pairing field would not be too strong at the nuclear surface. For that purpose, we used an additional scheme when constraining average pairing gaps. Since all our densities are expended in partial waves up to a given value ℓ_{max}, a pairing field strong at the surface is expected to give a significant change of the results if the maximum value of ℓ is changed from $\ell_{\text{max}} = \ell_0$ to $\ell_{\text{max}} = \ell_0 + 2$. Reciprocally, an average neutron pairing gap in a given nucleus, which is constrained to give approximately the same value for calculations with $\ell_{\text{max}} = \ell_0$ and $\ell_{\text{max}} = \ell_0 + 2$ can prevent the pairing field from being too strong near the surface.
  In practice, we constrained the average neutron pairing gap $\langle\Delta_n\rangle$ in ^{120}Sn calculated at $\ell_{\text{max}} = 9$ and $\ell_{\text{max}} = 11$. Pseudopotentials considered here lead to a low effective mass and thus a low density of states. In order to avoid too frequent collapses of pairing correlations in nuclei with subshells closure or with the opening of gaps for deformed nuclei, we decided to largely overshoot the value of the average pairing gap compared to what can be extracted from experimental mass staggering, and we used the target value of $\langle\Delta_n\rangle = 2.8$ MeV for the two values of ℓ_{max} with a small

uncertainty of 0.002 MeV. This ensures that the average pairing gap is almost the same for the two truncations and therefore the pairing field does not significantly change when more partial waves are added. The contribution from these constraints to the penalty function is denoted $\chi^2_{\rm gap}$.

- We have observed that the fit of the parameters can easily drive the pseudopotential into regions of the parameter space that lead to finite-size instabilities similar to those already identified for Skyrme functionals [26]. For this latter type of functionals, a tool based on the linear response theory was developed to characterize and avoid these finite-size instabilities. Such a tool does not yet exist for the pseudopotentials considered here, so we had to rely on an empirical criterion. We noticed that before the parameters of a pseudopotential get close to a region where finite-size isovector instabilities develop, strong oscillations can be seen in the isovector density $\rho_1(\mathbf{r})$ of heavy nuclei. Specifically, those oscillations lead to a decrease of the density of neutrons and increase of density of the protons at the centre of ^{208}Pb so that $\rho_1(0) < 0$. To avoid the appearance of the finite-size isovector instabilities, we introduced a constraint from the central isovector density $\rho_1(0)$ in ^{208}Pb to enforce $\rho_1(0) > 0$, that is, we have calculated the quantity,

$$C = \exp\left[-\frac{\rho_1(0)}{\alpha}\right], \tag{57}$$

which contributes to the penalty function as

$$\chi^2_{\rho_1} = \left(\frac{C - C^{\rm target}}{\Delta C}\right)^2, \tag{58}$$

with the targeted value of $C^{\rm target} = 0$ and the uncertainty $\Delta C = 1$. Parameter α was here empirically set to 0.006 fm^{-3}.

We note that the adopted structure of the penalty function mixes real experimental data and metadata, the latter certainly introducing some poorly controlled bias to the fit. Unfortunately, the use of metadata seems to be unavoidable, in the sense that the real experimental data do not alone constrain the model parameters sufficiently. As a result, without constraints on metadata, the fits easily drift towards clearly unphysical regions of the parameter space, and thus become useless. These aspects must become a centrepiece of future investigations in this domain.

5. Results and discussion

For the regularization ranges fixed at values between $a = 1.1$ and 1.3 fm, we minimised the penalty function defined in section 4.1. At NLO and N^{2}LO, this corresponds to a minimisation in 9- and 13-dimensional parameter space, respectively. In Fig. 1, we show the obtained values of the NLO and N^{2}LO penalty functions (56) as functions of a. As one could expect, the N^{2}LO penalty function is always lower than that at NLO. If we split different contributions to the penalty function, as defined in Eq. (56), we observe

Nucleus	$E_{\rm exp}$ [MeV]	$\Delta E_{\rm exp}$ [MeV]	$r_{\rm p}$ [fm]	$\Delta r_{\rm p}$ [fm]
^{40}Ca	-342.034	1.000	3.382	0.020
^{48}Ca	-415.981	1.000	3.390	0.020
^{56}Ni	-483.954	1.000	3.661	0.020
^{78}Ni	-641.743	2.000		
^{100}Sn	-824.775	1.000		
^{120}Sn	-1020.375	3.000		
^{132}Sn	-1102.680	1.000		
^{208}Pb	-1635.893	1.000	5.450	0.020

Table 1. Binding energies and proton radii used in the partial penalty functions $\chi^2_{\rm BE}$ and $\chi^2_{\rm rad}$, respectively. The binding energy of ^{78}Ni and the proton radius of ^{56}Ni are extrapolated values.

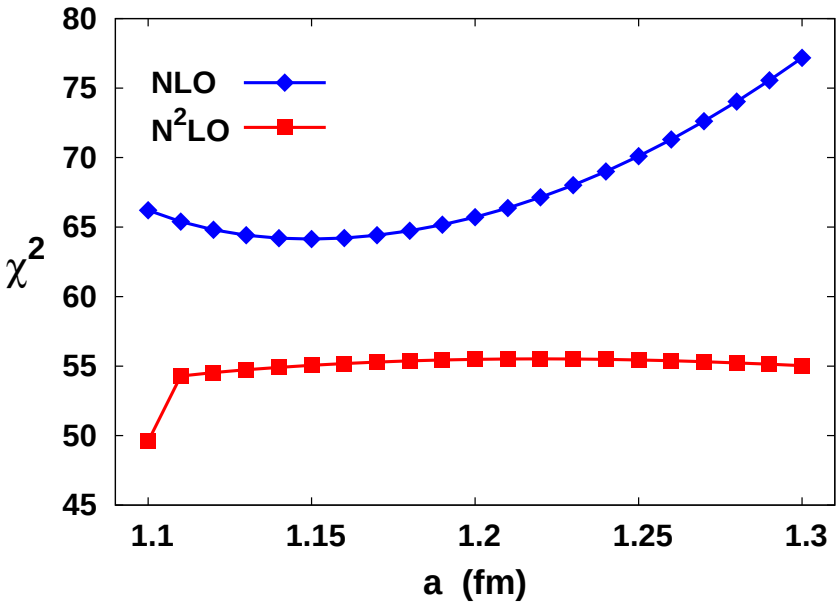

Figure 1. (Color online) The NLO and N^{2}LO penalty functions as functions of the regularization range a.

that the main improvement comes from the properties of the saturation point and from the gap in ^{120}Sn, see Table 2.

Table 2. Contributions to the penalty function, as defined in Eq. (56), along with its total value, shown at the regularization range of $a = 1.15\,$fm.

	$\chi^2_{\rm inm}$	$\chi^2_{\rm pol}$	$\chi^2_{\rm BE}$	$\chi^2_{\rm rad}$	$\chi^2_{\rm gap}$	$\chi^2_{\rho_1}$	χ^2
NLO	14.413	0.158	43.752	0.905	3.757	1.153	64.138
N^{2}LO	5.374	0.134	44.491	2.884	1.840	0.336	55.059

In the interval 1.1–1.3 fm, the NLO penalty function shows a significant dependence on the regularization range, whereas at N^{2}LO it is almost flat. This means that already at N^{2}LO, a change of the regularization range can be absorbed in the readjustment of coupling constants, as prescribed by the effective-theory approach [13].

At NLO, we were able to continue the minimisation to values of a well outside the interval 1.1–1.3 fm. However, at N^{2}LO, near $a = 1.1$ fm, we observe a sudden decrease of the penalty function. This decrease is accompanied by a strong readjustment of the coupling constants and a dramatic increase of the number of iterations needed to converge the HFB iterations for all nuclei. This trend becomes more pronounced for $a <$ 1.1 fm, and sometimes leads to impossibility to converge some of the HFB calculations defining the penalty function. We tentatively attribute these feature to the development of finite-size instabilities, which were not kept under control by the constraint on the isovector density in ^{208}Pb. We decided to leave any further investigation of this feature till when a linear response code is developed for finite-range EDF generators. Consequently, we did not continue to adjust the N^{2}LO pseudopotentials for shorter regularization ranges. We note here, that the appearance of instabilities at short regularization ranges may simply be the result of the parameter space being restricted by conditions (4), that is, by using local generators. Indeed, owing to these conditions, the Skyrme generators cannot be obtained by bringing to zero the regularization ranges of local generators (5) or (6). Therefore, studies in this limit are deferred till when restrictions to local generators are released.

Table 3. The NLO and N^{2}LO coupling constants of local pseudopotentials (3) and (7) regularized at $a = 1.15$ fm. (in MeV fm^{n+3}) shown together with their statistical errors.

Order	Coupling Constant	NLO REG2c.161026	N^{2}LO REG4c.161026
$n = 0$	$W_1^{(0)}$	41.678375±0.6	3121.637124±1.5
	$B_1^{(0)}$	−1405.790048±4.3	−4884.029523±1.8
	$H_1^{(0)}$	202.879894±4.1	3688.310059±2.9
	$M_1^{(0)}$	−2460.684507±6.7	−5661.028710±2.8
$n = 2$	$W_1^{(2)}$	−79.747992±4.2	547.802973±1.9
	$B_1^{(2)}$	73.112729±1.4	−319.513120±1.3
	$H_1^{(2)}$	−681.295790±3.2	−134.164127±0.3
	$M_1^{(2)}$	−48.161707±5.1	−318.407541±0.6
$n = 4$	$W_1^{(4)}$		2019.945667±2.2
	$B_1^{(4)}$		−2365.956384±1.6
	$H_1^{(4)}$		2310.445509±1.8
	$M_1^{(4)}$		−2117.509518±4.0
	$W_{\rm SO}$	177.076480±4.7	174.786236±5.1

The NLO and N^{2}LO coupling constants as functions of the regularization range a are plotted in the supplemental material [URL]. In the rest of this article, we discuss results obtained for $a = 1.15\,\mathrm{fm}$, which approximately corresponds to the minimum of the penalty function for the pseudopotential at NLO. Numerical unrounded values of the coupling constants at $a = 1.15\,\mathrm{fm}$ are listed in Table 3. Following the naming convention introduced in [15], we call parameter sets of regularized potentials as REGnx.DATE, where $n = 2p$ is the maximum order of higher-order differential operators used at N^{p}LO, letter "x" distinguishes different versions of the implementation, and "DATE" is a time stamp. In this study, we put x→c to mark the fact that the regularized potential is local, it is accompanied by zero-range two-body central and spin-orbit forces, and it is evaluated along with two-body centre-of-mass correction and exact direct and exchange Coulomb terms.

5.1. Infinite nuclear matter

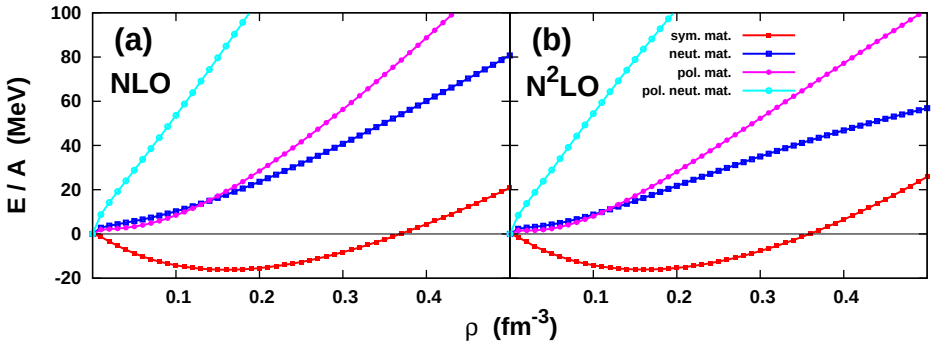

Figure 2. (Color online) Infinite-nuclear-matter equations of state for the NLO and N^{2}LO pseudopotentials at the regularization range of $a = 1.15\,\mathrm{fm}$.

Figure 2 shows the energy per nucleon for different states of infinite nuclear matter obtained with the pseudopotentials at NLO and N^{2}LO regularized at $a = 1.15\,\mathrm{fm}$. Near the saturation point, the two resulting equations of state are qualitatively similar. Nonetheless, for pure neutron matter and polarized symmetric matter, one can observe a trend that is significantly different for the high density part of the equations of state, where at N^{2}LO the energy per particle increases less rapidly. This high density region was not constrained, and it is not expected to have a sizable impact on properties of

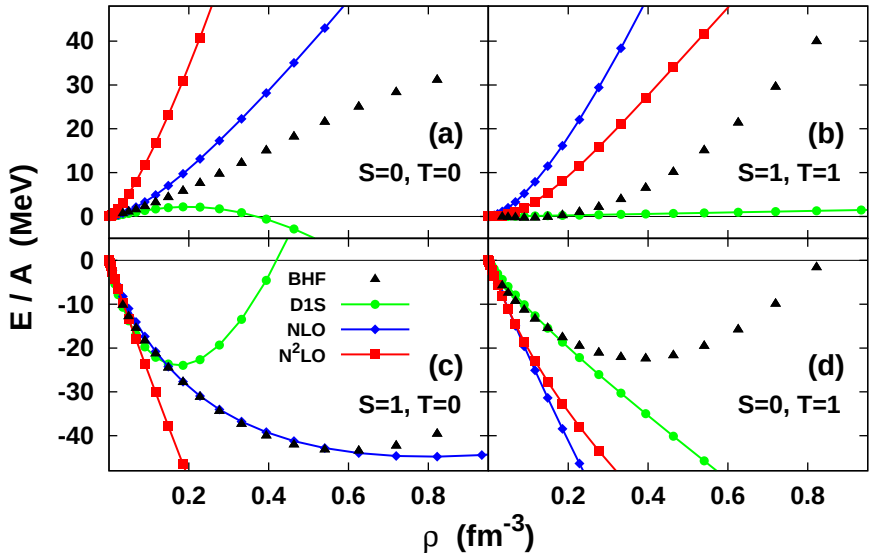

Figure 3. (Color online) Infinite-symmetric-nuclear-matter equation of state calculated for the NLO and N^{2}LO pseudopotentials at the regularization range of $a = 1.15\,\mathrm{fm}$ and split into four (iso)scalar/(iso)vector channels. Results are compared with those obtained for the Gogny D1S force [27] and Brueckner-Hartree-Fock (BHF) calculations of [28, 29].

finite nuclei. Similarities between the NLO and N^{2}LO equations of state partly come from strong constraints that were put on the properties of the saturation point. These properties are indeed well reproduced by the two pseudopotentials, see Table 4.

Table 4. Properties of the saturation point of infinite nuclear matter obtained for the NLO and N^{2}LO pseudopotentials regularized at $a = 1.15\,\mathrm{fm}$.

	ρ_{sat} (fm^{-3})	B (MeV)	K_∞ (MeV)	m^*/m	J (MeV)	L (MeV)
NLO	0.1599	-16.17	229.8	0.4076	31.96	64.04
N^{2}LO	0.1601	-16.09	230.0	0.4061	31.95	64.68

In Fig. 3, we show the NLO and N^{2}LO equation of state of infinite symmetric nuclear matter split into four (iso)scalar/(iso)vector channels. As discussed in [16], in principle the N^{2}LO pseudopotential can be accurately adjusted to reproduce all four channels simultaneously. In our case, because of the low effective mass, we had to overshoot the strength of the interaction in the scalar-isovector ($S = 0, T = 1$) channel, Fig. 3(d). As the sum of all four channels gives the constrained symmetric nuclear matter, equations of states in the $S = 0, T = 0$ and $S = 1, T = 1$ channels came out too high. Similarly as in [16], where an effective density-dependent term has been added on top of the N^{2}LO pseudopotential, we can expect that this unwelcome feature can be corrected in future

implementations involving a three-body force.

5.2. Statistical error analysis

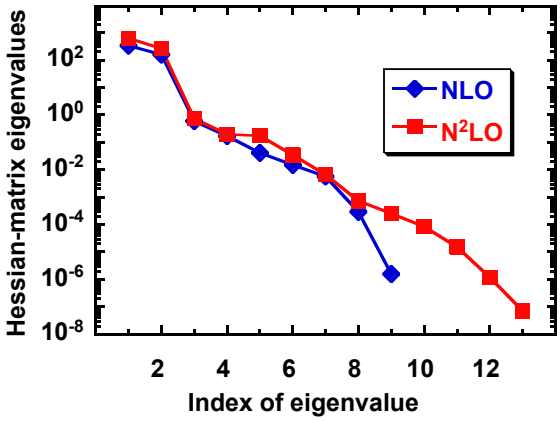

Figure 4. (Color online) Eigenvalues of the Hessian matrices calculated from the normalized penalty function for pseudopotentials at NLO and N^{2}LO with the regularization range of $a = 1.15\,\mathrm{fm}$.

For the two pseudopotentials built at NLO and N^{2}LO with regularization range $a = 1.15\,\mathrm{fm}$, we performed the analysis of statistical errors along the lines presented in [25]. For that purpose, we considered the scaled penalty function χ^2_{norm}, for which we calculated the Hessian matrix. Its eigenvalues are shown in Fig. 4. The total number of eigenvalues corresponds to the number of parameters allowed to vary during the fit, that is, to 9 for the pseudopotential at NLO and to 13 at N^{2}LO.

Eigenvalues of the Hessian matrix are indicative of how well the penalty function is constrained in those directions of the parameter space that are given by its eigenvectors. From the gap between the second and third eigenvalue it clearly appears that, irrespective of the order at which the pseudopotential is built, two such directions are well constrained. Beyond this second eigenvalue, the eigenvalues decrease in a fairly regular manner, and it is not possible to unambiguously define a dividing point between relevant and irrelevant eigenvalues. Furthermore, we have checked that the directions given by the eigenvectors of the Hessian matrix mix all the terms of the pseudopotential, so that no coupling constant (for the parametrization we have adopted) can be removed or frozen to get rid of a specific small eigenvalue.

The covariance matrix is the inverse of the Hessian matrix with a given number of its eigenvalues kept [25]. Its average value, calculated for a vector of derivatives of a given observable with respect to the parameters of the model, is called propagated error of the observable. In Fig. 5, we show such propagated errors determined for several observables in ^{120}Sn and ^{166}Er as functions of the number of largest eigenvalues kept in the spectrum of the Hessian matrix.

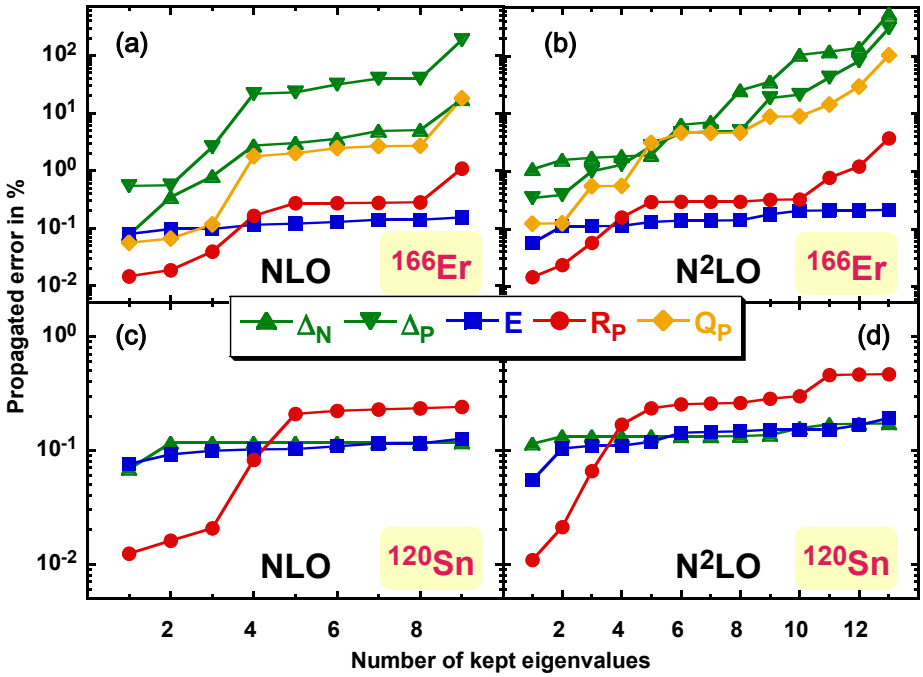

Figure 5. (Color online) Lower panels: Propagated errors of the total binding energies (E), average neutron pairing gaps (Δ_N), and proton rms radii (R_P) calculated for the spherical nucleus ^{120}Sn as a functions of the number of smallest eigenvalues kept in the spectrum of the covariance matrix. Upper panels: the same quantities supplemented with the proton average pairing gaps (Δ_P) and proton quadrupole moments (Q_P) calculated for the deformed nucleus ^{166}Er. All values are in per cent.

We see that for the two considered nuclei, the propagated errors are qualitatively similar when going from NLO to N^{2}LO. Errors of the total binding energies are generally small, of the order of 0.1 %, and do not show any significant dependence on the number of kept eigenvalues. For ^{120}Sn, the errors of the average neutron pairing gaps are similarly small and almost flat. This means that these observables, which were included in the definition of the penalty function, section 4.1, are insensitive to the unconstrained directions in the parameter space. Similarly, flatness of the propagated errors of the binding energy of ^{166}Er, which was not included in the penalty function, indicates that adding this one observable to the penalty function would not help in better constraining the model parameters.

The propagated errors of the proton rms radii are only about 0.01 % in the extreme case when only one eigenvalue is kept, and for five or more eigenvalues they reach what is approximately a plateau of 0.2–0.4 %. This means that directions in the parameter space that are associated with about five largest eigenvalues are meaningful, and should be included in the covariance matrix. Moreover, for ^{166}Er, the propagated errors of radii increase significantly when the last eigenvalue (NLO), or three last eigenvalues (N^{2}LO), are taken into account. This means that the current penalty function, which does not carry information concerning the structural properties of deformed nuclei, would be enriched by incorporating such information in future parameter adjustments. This

conclusion is substantiated by the propagated errors of quadrupole moments, which increase from 0.1 % to even 100 %.

The main, and striking, difference between the results obtained for ^{120}Sn and ^{166}Er concerns the average pairing gaps. As we already said, in ^{120}Sn, the propagated errors of the neutron gap are small and almost flat. However, in ^{166}Er, one sees a clear gradual increase of errors of pairing gaps with the number of kept eigenvalues. These large propagated errors are likely associated with the sensitivity of gaps to deformation. Indeed, changes of coupling constants induce changes of shape of the ^{166}Er ground state, and thus changes of its single-particle spectrum. This, in turn, can significantly modify the average pairing gaps and lead to large calculated propagated errors. Altogether, we conclude that adding to the penalty function data on spectroscopic properties of deformed nuclei may be more interesting from the point of view of constraining the model parameters than adding those related to their bulk properties like masses or radii.

For the following part of this article, to calculate the propagated errors, we chose to keep five largest eigenvalues of the Hessian matrices. This choice is based on the observation that beyond this point, several propagated errors, like those of radii, stop changing in a significant way. The corresponding covariance matrices are provided in the supplemental material [URL]. In Table 3 we show statistical errors of the coupling constants, which are equal to square roots of diagonal elements of the covariance matrices [25]. Note that in Table 3 we show unrounded values of the coupling constants, with several more digits beyond the statistically significant ones. Nevertheless, performing calculations with properly rounded values does change results, and significantly increases values of the penalty functions that move away from their minima. These changes are, of course, within bounds of propagated errors and thus are statistically insignificant, however, they also spoil smooth behaviour of observables and parameters as functions of the regularization range a. Therefore, in all calculations we recommend using the unrounded values of the coupling constants. Note also, that errors of parameters serve to illustrate the overall uncertainty of parameters only, whereas proper propagated errors of observables must be obtained by using the full covariance matrices.

5.3. Finite nuclei

In Fig. 6, we show ground-state energies of selected spherical nuclei obtained for the NLO and N^{2}LO pseudopotentials regularized at $a = 1.15\,\mathrm{fm}$. In addition to nuclei that were used to build the penalty function, results are shown for ^{44}Ca, ^{90}Zr, and ^{186}Pb. Apart from ^{48}Ca, ^{120}Sn, and ^{186}Pb, the agreement of the calculated binding energies with the experimental data is compatible with the calculated propagated errors. Large deviations obtained for two outliers, ^{120}Sn and ^{186}Pb, can most probably be related to the low effective mass and the resulting unrealistically small density of single-particle states. This is illustrated in Fig. 7, where we show proton and neutron single-particle

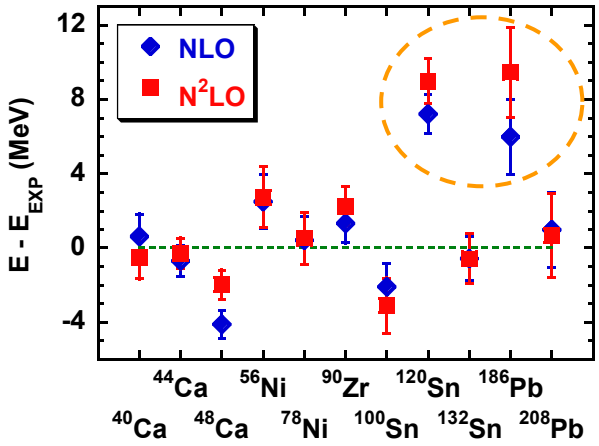

Figure 6. (Color online) Ground-state energies of selected spherical nuclei and their propagated errors calculated for the NLO and N^{2}LO pseudopotentials regularized at $a = 1.15\,\mathrm{fm}$, relative to experiment. The two open-shell outliers ^{120}Sn and ^{186}Pb (discussed in the text) are highlighted by the orange ellipse.

energies calculated in ^{208}Pb in comparison with the empirical values taken from Ref. [30].

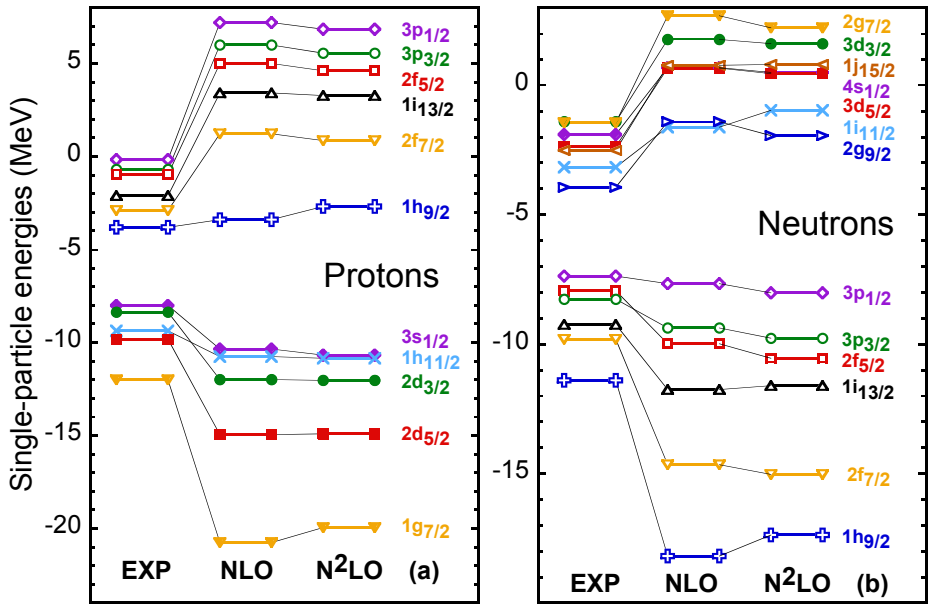

Figure 7. (Color online) Proton (left) and neutron (right) single-particle energies calculated in ^{208}Pb in comparison with the empirical values taken from Ref. [30] Note that states appearing at positive energies rather correspond to single-particle resonanses estimated by using the finite harmonic-oscillator basis.

As can be seen in Figs. 6 and 7, results obtained for both pseudopotentials are fairly similar, and we do not see any significant improvement when going from NLO to N^{2}LO. This is also visible in Table 2, where the decrease of the penalty function is

mostly related to the improvement of nuclear-matter properties.

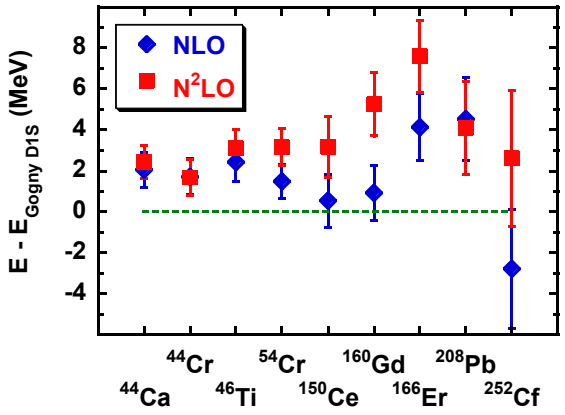

Figure 8. (Color online) Ground-state energies of selected spherical and deformed nuclei and their propagated errors calculated for the NLO and N^{2}LO pseudopotentials regularized at $a = 1.15$ fm, relative to those obtained for the Gogny D1S force [27].

Since our long term goal is to develop a pseudopotential for beyond mean-field calculation, a direct comparison of calculated mean-field binding energies with experimental data, as we did with Figure 6, only gives a partial information. It is of interest to compare the mean-field results with other calculations done at the same approximation from an effective interaction which is routinely used for mean-field calculations [31] and some beyond mean-field ones.

In Fig. 8 we compare ground-state energies calculated for the NLO and N^{2}LO pseudopotentials with those obtained for the Gogny D1S force [27]. These calculations were performed using finite harmonic-oscillator basis. Therefore, the results carry some trivial offset with respect to how the parameters were adjusted; nevertheless, the same basis was used for all three sets of calculations, and thus the relative energies are fully meaningful. We see that extrapolations to deformed nuclei, which were not included in the penalty function, work fairly well, although the propagated errors clearly increase with mass.

Finally, in Fig. 9, we plot the average neutron gaps calculated for the NLO and N^{2}LO pseudopotentials and the Gogny D1S force [27]. As anticipated by the constraint that we used for the neutron gap in ^{120}Sn in the penalty function, neutron gaps obtained for the pseudopotentials are fairly large, and almost for all nuclei considered here exceed those given by D1S. The primary goal of this preliminary study was to check if the form of the pseudopotential we develop allows us to generate interaction that is enough attractive in the particle-particle channel to lead to significant gaps. Fig. 9 shows that this goal was achieved. However, we also obtained proton gaps that often collapse in the deformed minima. This latter unwanted feature may once again be due to the low effective mass and too small density of single-particle energies.

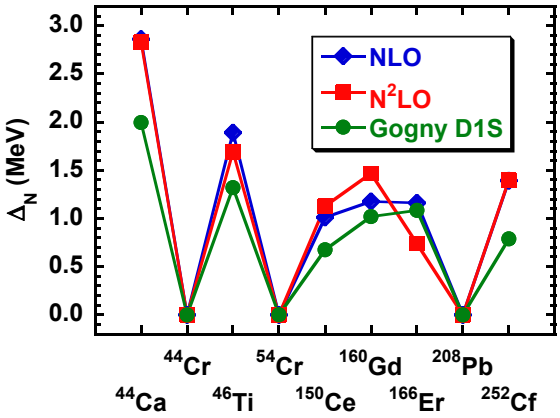

Figure 9. (Color online) Average neutron pairing gaps of selected spherical and deformed nuclei (their propagated errors are smaller than the symbols) calculated for the NLO and N^{2}LO pseudopotentials regularized at $a = 1.15$ fm, compared with those obtained for the Gogny D1S force [27].

6. Conclusions

In this article, we considered a local finite-range pseudopotential with a Gaussian regulator and derived its contributions to the particle-hole and particle-particle energies and to mean-field equations up to N^{2}LO. When supplemented with a zero-range two-body force acting in the particle-hole channel, it allowed us to build the first spuriousity-free nonlocal energy density functional that is capable of describing paired finite nuclei without using density-dependent terms.

To adjust the coupling constants of the pseudopotential, we defined a penalty function that constrained properties of selected spherical nuclei along with those of infinite nuclear matter. Its behaviour near the minimum allowed us to evaluate statistical errors of coupling constants and propagated errors of observables, including those for selected deformed nuclei. In this way, we were able to determine well and poorly constrained directions in the parameters space.

We consider the present parameterization to be an initial step towards a more definite solutions only. At present, the pseudopotential considered here gives low values of the effective mass, and consequently low densities of single-particle states in finite nuclei. In future implementations, we plan to correct for this by introducing three-body (or four-body) terms, eventually supplemented by velocity-dependent terms [32]. Our approach would then correspond to an extension of the interaction proposed by Onishi and Negele [33], who showed that it may have encouraging results for mean-field calculations.

The identified deficiencies of the NLO and N^{2}LO pseudopotentials derived in this work preclude using it within massive calculations that would produce masses and collective spectra across the Segré chart. We will undertake this task once we correct for this deficiencies, as mentioned above. Nevertheless, in Ref. [34] we present and discuss

results of calculations performed in semi-magic nuclei, and we refer the Reader to this publication for further information.

Acknowledgments

We wish to thank Marcello Baldo for providing us with his results from Brueckner-Hartree-Fock calculations of infinite nuclear matter and Michael Bender for a careful reading of this manuscript and helpful comments. K.B. thanks Tomás Rodriguez and Nicolas Schunck for useful discussions and benchmark calculations during the development of the code FINRES$_4$. This work was supported by the Academy of Finland and University of Jyväskylä within the FIDIPRO program, by the Royal Society and Newton Fund under the Newton International Fellowship scheme, by the CNRS/IN2P3 through PICS No. 6949, by the Polish National Science Center under Contract No. 2012/07/B/ST2/03907, and by the Academy of Finland under the Centre of Excellence Program 20122017 (Nuclear and Accelerator-Based Physics Program at JYFL). We acknowledge the CSC-IT Center for Science Ltd., Finland, for the allocation of computational resources.

References

[1] Skyrme T H R 1956 *Philosophical Magazine* **1** 1043–1054
[2] Skyrme T H R 1959 *Nuclear Physics* **9** 615 – 634 ISSN 0029-5582 URL http://www.sciencedirect.com/science/article/pii/0029558258903456
[3] Dechargé J and Gogny D 1980 *Phys. Rev. C* **21**(4) 1568–1593 URL http://link.aps.org/doi/10.1103/PhysRevC.21.1568
[4] Dobaczewski J, Stoitsov M V, Nazarewicz W and Reinhard P G 2007 *Phys. Rev. C* **76**(5) 054315 URL http://link.aps.org/doi/10.1103/PhysRevC.76.054315
[5] Anguiano M, Egido J and Robledo L 2001 *Nuclear Physics A* **696** 467 – 493 ISSN 0375-9474 URL http://www.sciencedirect.com/science/article/pii/S0375947401012192
[6] Bender M, Duguet T and Lacroix D 2009 *Phys. Rev. C* **79**(4) 044319 URL http://link.aps.org/doi/10.1103/PhysRevC.79.044319
[7] Tarpanov D, Toivanen J, Dobaczewski J and Carlsson B G 2014 *Phys. Rev. C* **89**(1) 014307 URL http://link.aps.org/doi/10.1103/PhysRevC.89.014307
[8] Skyrme T H R 1957 A nuclear pseudo-potential *Proc. of the Rehovot conference on nuclear structure* ed Lipkin H (North-Holland, Amsterdam, 1958) pp 20 – 25
[9] Raimondi F, Bennaceur K and Dobaczewski J 2014 *Journal of Physics G: Nuclear and Particle Physics* **41** 055112 URL http://stacks.iop.org/0954-3899/41/i=5/a=055112
[10] Dobaczewski J 2016 *Journal of Physics G: Nuclear and Particle Physics* **43** 04LT01 URL http://stacks.iop.org/0954-3899/43/i=4/a=04LT01
[11] Carlsson B G, Dobaczewski J and Kortelainen M 2008 *Phys. Rev. C* **78**(4) 044326 URL http://link.aps.org/doi/10.1103/PhysRevC.78.044326
[12] Raimondi F, Carlsson B G and Dobaczewski J 2011 *Phys. Rev. C* **83**(5) 054311 URL http://link.aps.org/doi/10.1103/PhysRevC.83.054311
[13] Dobaczewski J, Bennaceur K and Raimondi F 2012 *Journal of Physics G: Nuclear and Particle Physics* **39** 125103 URL http://stacks.iop.org/0954-3899/39/i=12/a=125103
[14] Sadoudi J, Bender M, Bennaceur K, Davesne D, Jodon R and Duguet T 2013 *Phys. Scr.* **T154** 014013 URL http://stacks.iop.org/1402-4896/2013/i=T154/a=014013

[15] Bennaceur, K, Dobaczewski, J and Raimondi, F 2014 *EPJ Web of Conferences* **66** 02031 URL http://dx.doi.org/10.1051/epjconf/20146602031
[16] Davesne D, Navarro J, Becker P, Jodon R, Meyer J and Pastore A 2015 *Phys. Rev. C* **91**(6) 064303 URL http://link.aps.org/doi/10.1103/PhysRevC.91.064303
[17] Perlińska E, Rohoziński S G, Dobaczewski J and Nazarewicz W 2004 *Phys. Rev. C* **69**(1) 014316 URL http://link.aps.org/doi/10.1103/PhysRevC.69.014316
[18] Bennaceur K *et al* 2017, to be submitted to Computer Physics Communications
[19] Hooverman R 1972 *Nuclear Physics A* **189** 155 – 160 ISSN 0375-9474 URL http://www.sciencedirect.com/science/article/pii/0375947472906501
[20] Dobaczewski J *et al* 2017, to be submitted to Computer Physics Communications
[21] Schunck N, Dobaczewski J, McDonnell J, Satua W, Sheikh J, Staszczak A, Stoitsov M and Toivanen P 2012 *Computer Physics Communications* **183** 166 – 192 ISSN 0010-4655 URL http://www.sciencedirect.com/science/article/pii/S0010465511002852
[22] Schunck N, Dobaczewski J, Satuła W, Bączyk P, Dudek J, Gao Y, Konieczka M, Sato K, Shi Y, Wang X B and Werner T R 2017 Submitted to Computer Physics Communications, arXiv:1612.05314v2 URL http://arxiv.org/abs/1612.05314v2
[23] JS Bell and THR Skyrme Phil Mag **1**, 1055 (1956)
[24] M Bender, K Rutz, P-G Reinhard and JA Maruhn 2000 *Eur. Phys. J. A* **7** 467–478 URL http://dx.doi.org/epja/v7/p467(epja219)
[25] Dobaczewski J, Nazarewicz W and Reinhard P G 2014 *Journal of Physics G: Nuclear and Particle Physics* **41** 074001 URL http://stacks.iop.org/0954-3899/41/i=7/a=074001
[26] Hellemans V, Pastore A, Duguet T, Bennaceur K, Davesne D, Meyer J, Bender M and Heenen P H 2013 *Phys. Rev. C* **88**(6) 064323 URL http://link.aps.org/doi/10.1103/PhysRevC.88.064323
[27] Berger J, Girod M and Gogny D 1991 *Computer Physics Communications* **63** 365 – 374 ISSN 0010-4655 URL http://www.sciencedirect.com/science/article/pii/001046559190263K
[28] Baldo M, Bombaci I and Burgio G F 1997 *Astron. Astrophys.* **328** 274–282
[29] Baldo M private communication
[30] Schwierz N, Wiedenhover I and Volya A 2007 arXiv:0709.3525 URL http://arxiv.org/abs/0709.3525
[31] Hilaire S and Girod M URL http://www-phynu.cea.fr/science_en_ligne/carte_potentiels_\microscopiques/ca
[32] Sadoudi J, Duguet T, Meyer J and Bender M 2013 *Phys. Rev. C* **88**(6) 064326 URL http://link.aps.org/doi/10.1103/PhysRevC.88.064326
[33] Onishi N and Negele J 1978 *Nuclear Physics A* **301** 336 – 348 ISSN 0375-9474 URL http://www.sciencedirect.com/science/article/pii/037594747890266X
[34] Bennaceur K, Dobaczewski J and Gao Y 2017 arXiv:1701.08062 URL http://arxiv.org/abs/1701.08062